nature communications

Article

https://doi.org/10.1038/s41467-025-59180-9

Scaled CO Electroreduction to Alcohols

Received: 8 July 2024

Accepted: 14 April 2025

Published online: 29 May 2025

Check for updates

Panagiotis Papangelakis[1,7], Colin P. O'Brien[1,2,7], Ali Shayesteh Zeraati[1,3,7] ✉, Shijie Liu[1], Alexander Paik[4], Vivian Nelson[1], Sungjin Park[5], Yurou Celine Xiao[1], Roham Dorakhan[5], Puhua Sun[1], Jinhong Wu[1], Christine M. Gabardo[2], Ning Wang[5], Rui Kai Miao[1], Edward H. Sargent[5,6] & David Sinton[1] ✉

Electrocatalysis offers a promising route to convert CO_2 into alcohols, which is most efficient in a two-step cascade reaction with CO_2-to-CO followed by CO-to-alcohol. However, current alcohol-producing CO_2/CO electrolyzers suffer from low selectivity or alcohol crossover, resulting in alcohol concentrations of less than 1%, which are further diluted in downstream cold-traps. As a result, electrocatalytic alcohol production has yet to be scaled beyond the lab (1-10 cm^2). Here, we reverse the electroosmotic drag of water using a cation exchange membrane assembly, enabling the recovery of over 85% of alcohol products at a concentration of 6 wt.%. We develop a multi-step condenser strategy to separate the produced alcohols from the effluent gas stream without dilution. Scaling up this approach to an 800 cm^2 cell resulted in an output of 200 mL alcohol/day.

The electrosynthesis of ethanol through carbon dioxide reduction reactions (CO_2R) provides a potential carbon-neutral pathway for converting intermittent renewable energy into liquid products that are storable and shippable[1–5]. Ethanol (C_2H_5OH) and n-propanol (C_3H_7OH) have been identified as particularly appealing electrolysis products in this regard, in view of their market size and carbon intensity[6]. The conventional approach to ethanol production is carbon-intensive, as life-cycle assessments indicate a carbon intensity of bioethanol exceeding that of conventional gasoline, thus motivating the development of low-carbon alcohol production pathways[7]. While bio-electrochemical and thermochemical methods are capable of upgrading CO_2 to ethanol and other multicarbon products, they suffer from lower efficiencies or higher carbon footprints compared to electrochemical production[8–13].

Recent advances in gas diffusion electrodes (GDEs), electrolyzer design, and catalysts have enabled the production of alcohols with a high faradaic efficiency (FE)[14–17] while operating at industrially relevant current densities (>100 mA/cm^2)[6,18]. However, these systems are not suited for scale-up due to a combination of crossover of produced alcohol to the anode electrolyte, low single-pass conversion efficiency (SPCE), and low energy efficiency (EE)[19].

In traditional membrane electrode assemblies (MEAs) equipped with an anion exchange membrane (AEM), up to 80% of alcohols cross the AEM to the anolyte[20] via diffusion[21] and electroosmotic drag[22–24]. This crossover risks the oxidation of produced alcohols to acetate or CO_2, and the alcohols that remain are diluted (to ~0.05 wt.%) in the anolyte[25]. Alcohols in such low concentrations cannot be economically recovered, because the energy cost for purification would exceed the energy content of the alcohols by more than an order of magnitude[25,26]. Strategies to collect concentrated alcohols with low crossover rates typically require multi-membrane or solid-state electrolyte systems prone to high cell voltages (>3 V)[20,25,27,28] and limitations in SPCE (CO_2 utilizations <25%)[29–34]. The complexity of such multi-membrane systems poses an additional barrier to scaling, which is a challenge that demands electrocatalytic routes to concentrated alcohols without compromising SPCE or EE.

Cascade electroreduction of CO_2 to CO followed by carbon monoxide reduction (COR) offers high overall SPCE and energy efficiency. This approach takes advantage of comparably mature and

[1]Department of Mechanical and Industrial Engineering, University of Toronto, Toronto, ON, Canada. [2]CERT Systems Inc, 501 Alliance Avenue, Suite 406, Toronto, ON, Canada. [3]Acceleration Consortium, University of Toronto, Toronto, ON, Canada. [4]Department of Chemical Engineering and Applied Chemistry, University of Toronto, Toronto, ON, Canada. [5]Department of Electrical and Computer Engineering, University of Toronto, Toronto, ON, Canada. [6]Department of Electrical and Computer Engineering, Northwestern University, Evanston, IL, USA. [7]These authors contributed equally: Panagiotis Papangelakis, Colin P. O'Brien, Ali Shayesteh Zeraati. ✉e-mail: ali.shayesteh@utoronto.ca; sinton@mie.utoronto.ca

efficient CO_2-to-CO electrolyzers, such as solid oxide electrolyzer cells (SOECs), followed by CO reduction to multicarbon products in a dedicated electrolyzer[35,36]. This approach also avoids the issue of reactant CO_2 loss to carbonate formation, which is typical of one-step CO_2R electrolyzers. Since CO does not form carbonates, COR systems can operate with alkaline electrolytes at both the anode and cathode, minimizing the cathode overpotential and Nernstian pH gradient potential. Previous studies combining SOECs with COR demonstrated CO-to-C_2H_4 electrolyzers with 20% EEs and superior SPCEs compared to CO_2R systems[37].

Despite progress in reducing CO to multicarbon products such as ethylene[38,39] and acetate[40–42], high-concentration, low-crossover CO-to-alcohols electrolyzers have yet to be produced at a relevant scale[43–45]. Electrodes for CO-to-alcohol systems are currently limited in size to <5 cm^2 [14,17,46,47], while CO-to-acetate systems have achieved scales upward of 100 cm^2 for individual cells[42]. In addition, the method to collect and measure alcohols from the gas outlet in both COR and CO_2R systems dilute the final alcohol product in water-filled cold-traps. This method enables the measurement of the pre-diluted alcohol concentration but prevents scaled production, which requires the product in concentrated form.

Here, we report large-scale electrocatalytic alcohol production from CO at high recovery rates. We prevented the dilution of alcohols observed in conventional AEM electrolyzers by reversing the ion flow and the associated electroosmotic water flux. Using a cation exchange membrane (CEM) electrolyzer, we collected > 85% of alcohols produced by COR from the cathode gas outlet. Scaling this approach from 5 to 50 cm^2 highlighted the limitation of the conventional cold-trap method for capturing the alcohol products. To address this, we developed a scalable multi-step condensation strategy that recovers 95% of alcohols from the effluent gas stream at viable concentrations, without dilution. We further demonstrated the scalability by operating an 800 cm^2 cell, which is the largest single COR electrolyzer to date[42], with an output of 200 mL of alcohol per day. Our approach enabled stable alcohol electrosynthesis for over 100 hours. With a stable, large area cell, this work provides a model for scaled alcohol electroproduction.

Results

Alcohol production and crossover investigation

We sought first to understand how membranes affect alcohol production and crossover in COR MEA electrolyzers. We began by assembling an AEM (PiperION-40 μm) MEA and a CEM (Nafion 1110) MEA with cathodes consisting of a high PTFE content gas diffusion layer (GDL) and a catalyst of sprayed CuO nanoparticles (CuONP) (Fig. 1A and B). A high PTFE content was used to prevent flooding of the electrolyzer due to excess water from the CEM[48]. These tests employed a commercial CuO NP catalyst in a standard MEA electrolyzer. We selected the PiperION AEM for its low water uptake, which reduces electroosmotic drag from the cathode to anode to minimize the alcohols transported to the anolyte. For the CEM MEA electrolyzer, we selected a thick Nafion membrane with low water transport (1110 CEM) to minimize the electroosmotic drag of water from the anode-to-cathode that can dilute the alcohols. This configuration limits the

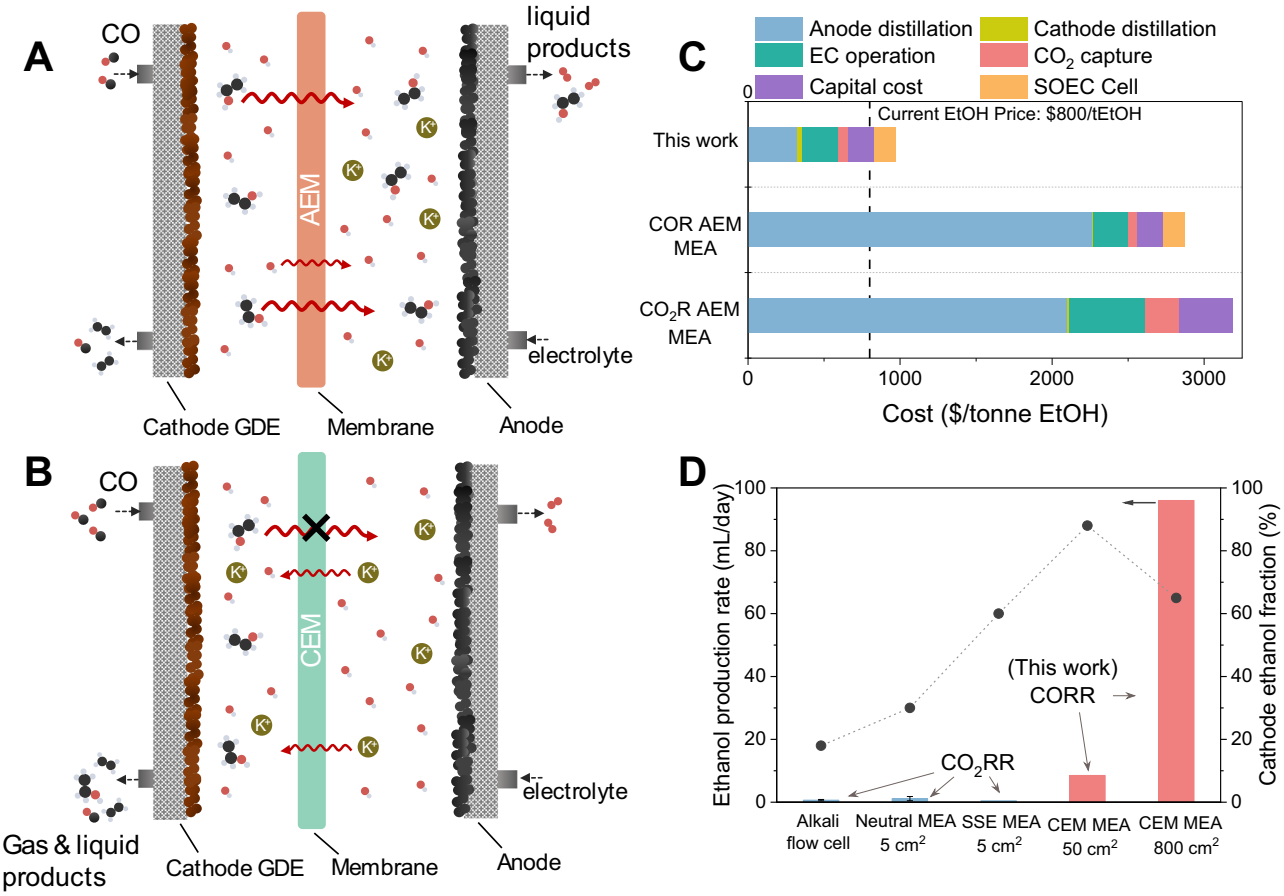

Fig. 1 | COR to alcohol performance in different electrolyzers. Schematics of COR in (**A**) AEM MEA and (**B**) CEM MEA showing the main charge carriers and the location where most of the liquid products are detected. Red = oxygen; black = carbon; grey = hydrogen; green = potassium. **C** TEA analysis comparing our strategy to typical CO AEM and CO2 AEM systems at ideal performance metrics. **D** The SSE MEA refers to our previous work on producing concentrated ethanol directly from a CO2 MEA electrolyzer[25]. The values are presented in Supplementary Table 11. Source data for the results are provided as a Source Data file.

diffusion of alcohols through the membrane and reduces electro-osmotic drag of water from the anolyte, enabling high cathodic alcohol concentrations.

While both cells demonstrated a similar product distribution, the CEM electrolyzer produced a higher total alcohol FE of 35%, compared to 24% alcohol FE with the AEM electrolyzer, at a current density of 200 mA/cm^2 (Supplementary Fig. 1A). We chose a current density of 200 mA/cm^2 because higher current densities are preferable for industrial application[2]. The difference in alcohol FE of the CEM electrolyzer is due to the elevated hydroxide and cation concentration at the cathode, which enhances CORR rate and reduces the hydrogen evolution reaction (HER). The negatively charged CEM retains OH^- ions at the cathode and facilitates the transport of cations from the anolyte, increasing the cation concentration and stabilizing active intermediates in the CORR process[49–51]. Furthermore, the CEM electrolyzer suffered less alcohol crossover, retaining > 85% of the generated alcohols on the cathode side, compared to only 16% with the AEM electrolyzer (Supplementary Fig. 1B). We attributed this difference in alcohol crossover between the AEM and CEM to reversing the direction of electroosmotic drag, which served to block advective and diffusive transport of ethanol from the cathode to the anode (Fig. 1A and B). The CEM MEA had a higher full-cell potential of -2.58 V compared to -2.47 with the AEM MEA due to greater ohmic resistance from the thicker membrane (254 μm vs. 40 μm). Electrochemical impedance spectroscopy (EIS) showed series resistance (Rs) values of 0.45 Ω for the AEM MEA and 1.13 Ω for the CEM MEA (Supplementary Fig. 2). Despite the higher voltage, the CEM outperforms the AEM in terms of alcohol retention on the cathode-side, with an $EE_{alcohol\text{-}cathode}$ of 10%, compared to 2% for the AEM.

We further explored the effect of electroosmotic drag in control experiments where we added 4 wt.% ethanol to the catholyte and operated the cathode under hydrogen evolution reaction at 200 mA/cm^2 (Supplementary Fig. 3). We measured the drop in ethanol concentration after 5 hours of operation, with or without current, to quantify ethanol crossover caused by electroosmotic drag. We did not measure ethanol concentration in the anolyte as oxidation to acetate or CO_2 occurs[25]. Applying current decreased cathode-side ethanol concentration in the AEM system, while it increased in the CEM system compared to no current. These results indicate that the direction of ion flow modulates ethanol crossover. The CEM also reduced alcohol crossover without current, likely due to its greater thickness[52,53].

We then investigated the effect of the CEM thickness on alcohol crossover and electrolyzer performance (Supplementary Fig. 4). Reducing the membrane thickness from 254 μm to 127 μm decreased the full-cell voltage by up to 0.08 V, reaching a value of −2.5 V, comparable to the AEM MEA. However, the thinner Nafion 115 membrane retained nearly 10% less alcohol at the cathode side compared to the thicker Nafion 1110, consistent with previous studies showing higher alcohol crossover in thinner CEMs[53]. This highlights a trade-off between cell voltage and alcohol crossover with membrane thickness.

Increasing the applied current density in both the AEM and CEM MEAs revealed a shift in alcohol selectivity from propanol to ethanol (Supplementary Figs. 5 and 6). Furthermore, alcohol crossover increased with current density in the AEM MEA, while the effect was less pronounced in the CEM MEA. The increase in alcohol crossover in the AEM MEA highlights the effect of electroosmotic drag, where the water flux from the anode to the cathode increases with the applied current, transferring more alcohol to the anolyte. The effect is less pronounced in the CEM MEA likely due to the already low degree of alcohol crossover at the measured currents.

We performed a technoeconomic analysis that revealed alcohol dilution due to crossover in the AEM system, both in COR and CO_2R configurations, increased the downstream separation costs by sevenfold (Fig. 1C, Supplementary Note 1, Supplementary Figs. 7 and 8). Testing the CEM MEA with a CO_2 feed revealed an HER of > 90% due to immediate salt precipitation at the cathode[54], suggesting that the single-membrane CEM configuration is uniquely suited to CO feeds (Supplementary Fig. 9). Compared to other CO_2 electrolyzers targeting alcohol production, the CEM CO electrolyzer used in this work achieves greater alcohol recovery at the cathode side and does so in a simple single-membrane configuration that is easier to scale (Fig. 1D, Supplementary Note 2). Moreover, comparing the CEM MEA to previous alcohol-producing systems revealed a lower total production energy cost due to the lower voltage and alcohol crossover achieved in the single membrane system (Supplementary Tables 10 and 11). We concluded that this single-membrane CEM CO electrolyzer model is currently the most suitable for scaling.

Optimization of the 1 cm^2 Cell

To minimize the energy cost of product separation, it is crucial to maximize the amount of alcohols recovered from the cathode gas outlet at the highest possible concentration (Fig. 1C). Previous CO_2R AEM systems employed elevated temperatures to enhance alcohol evaporation into the cathodic gas stream[25]. The increased vapor pressure of alcohols at higher temperatures increased alcohol concentration and reduced alcohol crossover to the anode side. Here, in the COR CEM MEA electrolyzer, we found that increasing the temperature from 20 °C to 50 °C did not have a significant influence on the alcohol FE or crossover (Fig. 2A). However, the increase in cell temperature resulted in less-concentrated alcohol on the cathode side (Fig. 2B). Higher cell temperatures increase the membrane's water uptake[55], which can induce more water electroosmotic drag from the anode to the cathode. The increased water uptake leads to greater evaporation of water from the cathode at higher temperatures, diluting the alcohol condensed from the outlet gas. However, the increased water uptake did not lead to higher alcohol crossover, as it is counter to the direction of alcohol transport in the CEM architecture.

Controlling the gas flow rate is another means of influencing the outlet alcohol concentration[23]. We found that increasing the gas flow rate from 10 sccm to 50 sccm doubled the cathodic alcohol concentration to 6 wt.%, while improving FE and decreasing crossover (Fig. 2C and D). We attributed the increase in cathodic ethanol concentration to higher alcohol vaporization rates caused by increased convective mass transfer at higher carrier gas (CO) flowrates (Fig. 2E). While increasing gas flowrate lowers carbon conversion efficiency (CE), bypassing this issue is possible by condensing the alcohol products and recirculating the outlet gas for multiple passes, which is an advantage unique to the phase-separable mixtures of reactant and product.

Scaling to 50 cm^2 at high recovery rates

We scaled the CEM CO electrolyzer initially to 50 cm^2. To simulate industrial-scale separation for alcohol production, we examined the feasibility of employing a condenser to collect the produced alcohols on the cathode side to avoid the limitations posed by conventional cold-trap liquid collectors. Although dilution cold-traps are convenient in laboratory-scale settings, they dilute the generated alcohols by adding excess water during the bubbling step. This lowers the alcohol concentration by an order of magnitude after product collection and may introduce more error in the measurement (Supplementary Note 3). We ran an initial experiment at 200 mA/cm^2 using a single low-temperature condenser at 10 °C. We observed a large drop in alcohol FE compared to a 5 cm^2 bench-scale test with the liquid-collector (Fig. 3A and Supplementary Fig. 10). We posited that the missing FE was due to the single condenser failing to trap all the alcohol products. We tested this hypothesis by simulating the condensation of the generated alcohols in Aspen Plus (Supplementary Note 4 and Supplementary Fig. 11). We found that approximately 30% of cathodic ethanol cannot be trapped in the single 10 °C condenser due to the high flow rate of the carrier CO gas and the vapor pressure of ethanol.

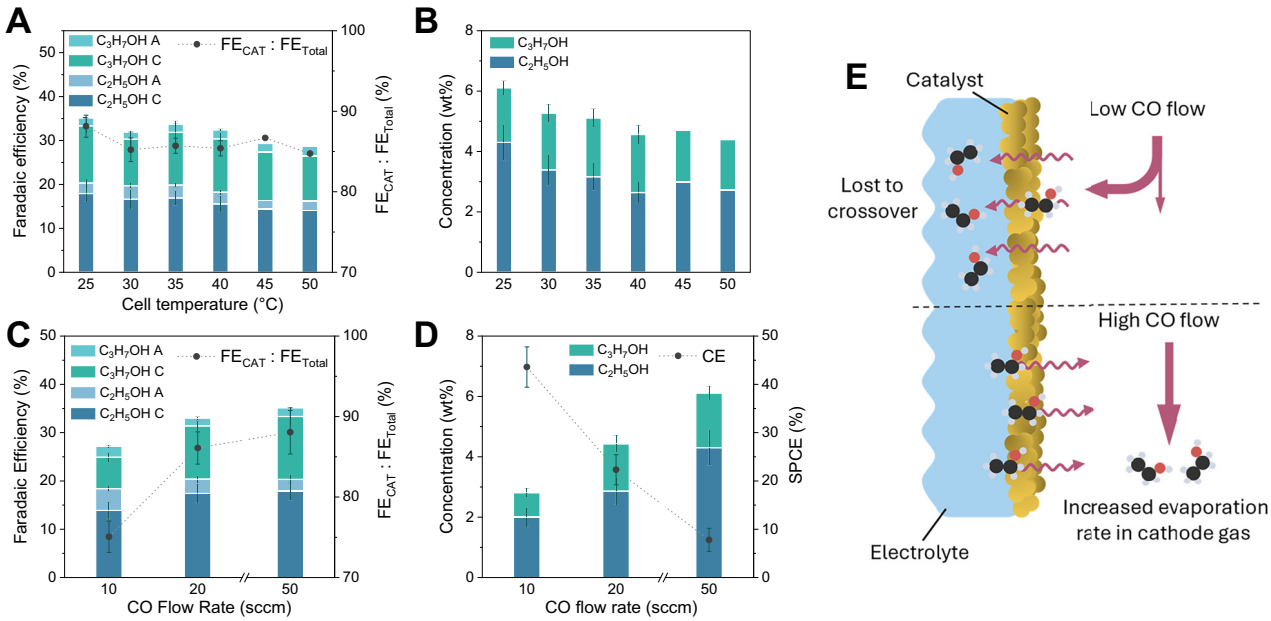

Fig. 2 | The effect of temperature and CO flow rate on CEM MEA cell performance at 200 mA/cm². **A** The alcohol FE distribution and crossover as functions of the cell temperature. The secondary axis depicts the ratio of alcohols collected on the cathode to the total amount of alcohols (alcohol crossover). Products marked with a C are from the cathode gas outlet, and those marked with an A are from the anolyte. **B** The alcohol concentration collected in the cold-trap at the cathode gas outlet relative to cell temperature. **C** The alcohol FE distribution and crossover as functions of the CO flow rate. **D** The alcohol concentration and carbon efficiency concerning the input CO flow rate. **E** Schematic illustrating reduced alcohol crossover with increasing inlet CO flow rate. Red = oxygen; black = carbon; grey = hydrogen; yellow = copper. Where error bars are shown, values are means, and error bars indicate s.d. ($n = 3$ replicates). The source data for the results is provided as a Source Data file.

Since a high flow rate is needed to minimize alcohol crossover, a method to condense alcohol while still maintaining a high flow rate CO stream was required.

We hypothesized that the residual alcohols could be recovered by introducing a second downstream condenser at a lower temperature (Fig. 3B). We conducted simulations with the second condenser at various inlet flowrates to determine the fraction of total ethanol in the outlet stream that would be condensed, depending on the temperature of the second condenser (Fig. 3C). We found that a second condenser with a temperature < -30 °C is needed to condense 95% of the ethanol in the outlet gas stream at these conditions.

We replicated the 50 cm² experiment using the two-stage condenser strategy. The first condenser remained at 10 °C, while we kept the second at −78 °C by immersing it in a bath with a dry ice/isopropanol mixture, ensuring the condensation of all alcohols. The first condenser removed most of the water and prevented freezing in the second condenser. The FE for all products reached 98%, with a total alcohol FE of approximately 28%, mirroring the results of the benchscale test (Fig. 3D and Supplementary Fig. 10). The second condenser produced a stream of 28 wt.% ethanol and 20 wt.% propanol, summing up to 48 wt.% for all alcohols (Fig. 3E). Thus, the two-stage condenser strategy both eliminates the water dilution step, allowing alcohols to be captured at a higher concentration, and improves the overall alcohol recovery. A subsequent energy analysis indicates that the energy cost of operating a second condenser is small (<-3% of total energy input, Supplementary Note 5). This approach can be readily scaled to collect concentrated alcohols produced by much larger electrolyzers.

Demonstration at 800 cm²

Building upon the outcomes from the 50 cm² testing, we scaled up the electrolyzer size to 800 cm², which is suitable for stacking in industrial applications and compatible with currently available commercial membranes (Fig. 4A, Supplementary Figs. 12 and 13). Further details on the design of the 800 cm² cell can be found in an earlier study[56]. Due to the large amount of water expected to be transported to the cathode via electroosmotic drag, we added a third pre-condenser stage at room temperature (20 °C) to remove the excess water. The electrolyzer operated at a lower current density of 100 mA/cm² compared to the previous test due to limitations of the mass flow controller, increasing propanol FE to 18.5%. We achieved an ethanol FE of ~19%, similar to the 5 cm² and 50 cm² electrolyzer (Fig. 4B). The 800 cm² electrolyzer experienced greater alcohol crossover to the anolyte, with approximately 65% of alcohols retained at the cathode outlet, compared to ~88% for the 5 cm² and 50 cm² cells. We attributed the increased alcohol crossover in the 800 cm² electrolyzer to the higher feed-gas pressure, as the flow field design in the larger electrolyzer was not optimized to maintain the same pressure drop as in the smaller electrolyzers, with an overall pressure drop of 10 psi. This higher feed-gas pressure resulted in greater alcohol transport across the membrane and less ethanol evaporation, leading to greater alcohol crossover (Supplementary Fig. 14). Improvements in pressure distribution on both sides of the MEA were needed to reduce pressure gradients. After adding the room-temperature condenser, both the 10 °C and −78 °C condensers collected higher alcohol concentrations (~40 wt.%), as most of the water was removed in the first stage (Fig. 4C). The 800 cm² electrolyzer demonstrated a production rate of 96 mL/day of ethanol and 84 mL/day of propanol (Fig. 4D). To our knowledge, this system represents the largest-single cell COR demonstration, for any product, to date[42]. The 800 cm² cell operated for two hours with no measurable change in performance and produced 15 mL of alcohol during that run time.

To establish the stability of the CEM electrolyzer, we conducted a test with the 5 cm² cell over a longer duration. The system maintained a total alcohol FE of ~35% at a full-cell potential of around −2.4 V for more than 100 hours (Fig. 4E and Supplementary Table 15). The alcohol concentration remained stable, averaging around 6 wt.%, with over approximately 84% of the alcohols extracted from the cathode side,

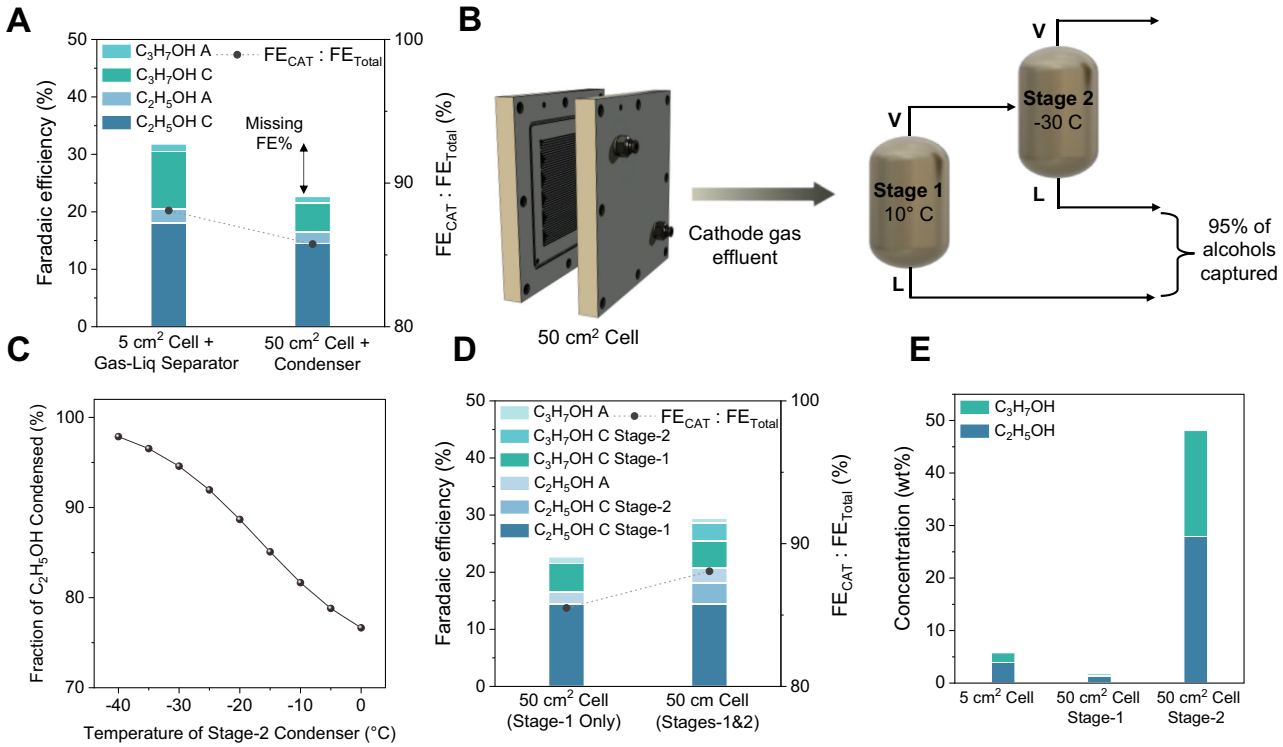

Fig. 3 | Ethanol production with 50 cm² electrolyzer. A The distribution of alcohol FE and crossover as functions of the electrolyzer size and alcohol separation method. **B** Diagram illustrating the placement of two condensers downstream of the cathode gas outlet. The symbols V & L represent the vapor and liquid outlets from the condensers, respectively. **C** Results from the Aspen Plus simulation showing the fraction of ethanol condensed from a stream containing CO, gas products, and water vapor. **D** Alcohol FE distribution and crossover as functions of the number of condensers applied to the cathode gas outlet. Products marked with a stage-1 indicate products collected from the first condenser, products marked with a stage-2 indicate products collected from the second condenser, and products marked with an A indicate those collected from the anolyte. **E** The concentration of alcohols collected from the 5 cm² electrolyzer set up, which includes only 1 condenser, and the concentration of alcohols collected from the first and second stage condensers are applied to the 50 cm² cell. The source data for the results are provided as a Source Data file.

indicating the potential for long-term COR-based production of alcohol. To further validate the long-term operation of the large-scale electrolyzer, we operated the 800 cm² electrolyzer for an additional 7.5 hours (Supplementary Fig. 15 and Supplementary Table 16), which is the maximum allowable duration due to lab restrictions preventing the use of high CO flow rates for longer durations. We observed no considerable changes in the catalyst structure or ionomer binder after this stability test (Supplementary Figs. 16 and 17). We also observed no significant degradation in alcohol FE or crossover, supporting the scalability of the CEM MEA for large-scale alcohol production from CO.

Discussion

We developed a scalable COR electrolyzer that produces CO_2-derived alcohols with lower energy intensity. We found that the conventional AEM MEA diluted the alcohol products due to electroosmotic drag, which we mitigated by reversing the ion flow using a CEM MEA to minimize alcohol crossover. Optimization tests on the CEM MEA demonstrated that increasing the CO flow rate enhanced alcohol recovery, achieving over 85% recovery from the cathode side at concentrations up to 6 wt.%. Scaling to a 50 cm² electrolyzer initially led to significant product loss due to high feed gas flow rates, which required us to add a second low-temperature condenser, which captured over 95% of alcohols from the gas phase. Experimental validation confirmed concentrations up to 48 wt.% using the second condenser. We achieved further scalability validation by operating an 800 cm² electrolyzer, where most of the alcohols remained on the cathode side and were effectively extracted from the cathode outlet using a multi-stage condenser strategy. Additionally, the optimized CEM electrolyzer configuration demonstrated more than 100 hours of stability when applied to the 5 cm² cell, maintaining low alcohol crossover rates. This represents the largest COR cell to date, validating industrial-scale COR for alcohol production.

Methods

Gas diffusion electrode preparation

The gas diffusion electrodes were prepared by spraying a catalyst layer onto a custom high PTFE content gas diffusion layer. A CuO nanoparticle catalyst ink was prepared by mixing 200 mg of CuO nanoparticles (Sigma Aldrich, 544868), 150 mg of Nafion D521 dispersion (Fuel Cell Earth, D521), 150 mg of PTFE nanoparticles (100 nm), and 36 mL of methanol. The catalyst nanoparticle ink was sonicated for 2 h in an ultrasonic bath and spray-coated onto a 50 cm² custom GDL with an airbrush until a loading of 1.5 mg/cm² was reached. The ink was altered proportionally for the 800 cm² test.

The custom gas diffusion layer preparation is based on our previous report[48]. Briefly, a carbon slurry was prepared by mixing 0.5 g of carbon black (Alfa Aesar, 39724) with 5 drops of Triton X-100 (Sigma Aldrich, X100) and 35 mL of isopropyl alcohol. A PTFE dispersion was made by diluting 5 g of a commercial PTFE dispersion (Sigma Aldrich, 665800) with 5 g of DI water. The slurry and dispersion were mixed, combined, and blade-coated onto a wet-proofed carbon paper (Fuel Cell Earth MGL190, 50% wet proofed, 80190 T) using a blade height of 0.6 mm. The gas diffusion layers were then heat-treated in a furnace at 180 °C for 3 h, at 280 °C for 3 h, and 340 °C for 1 h to remove solvents, surfactants, and sinter the PTFE.

https://doi.org/10.1038/s41467-025-59180-9

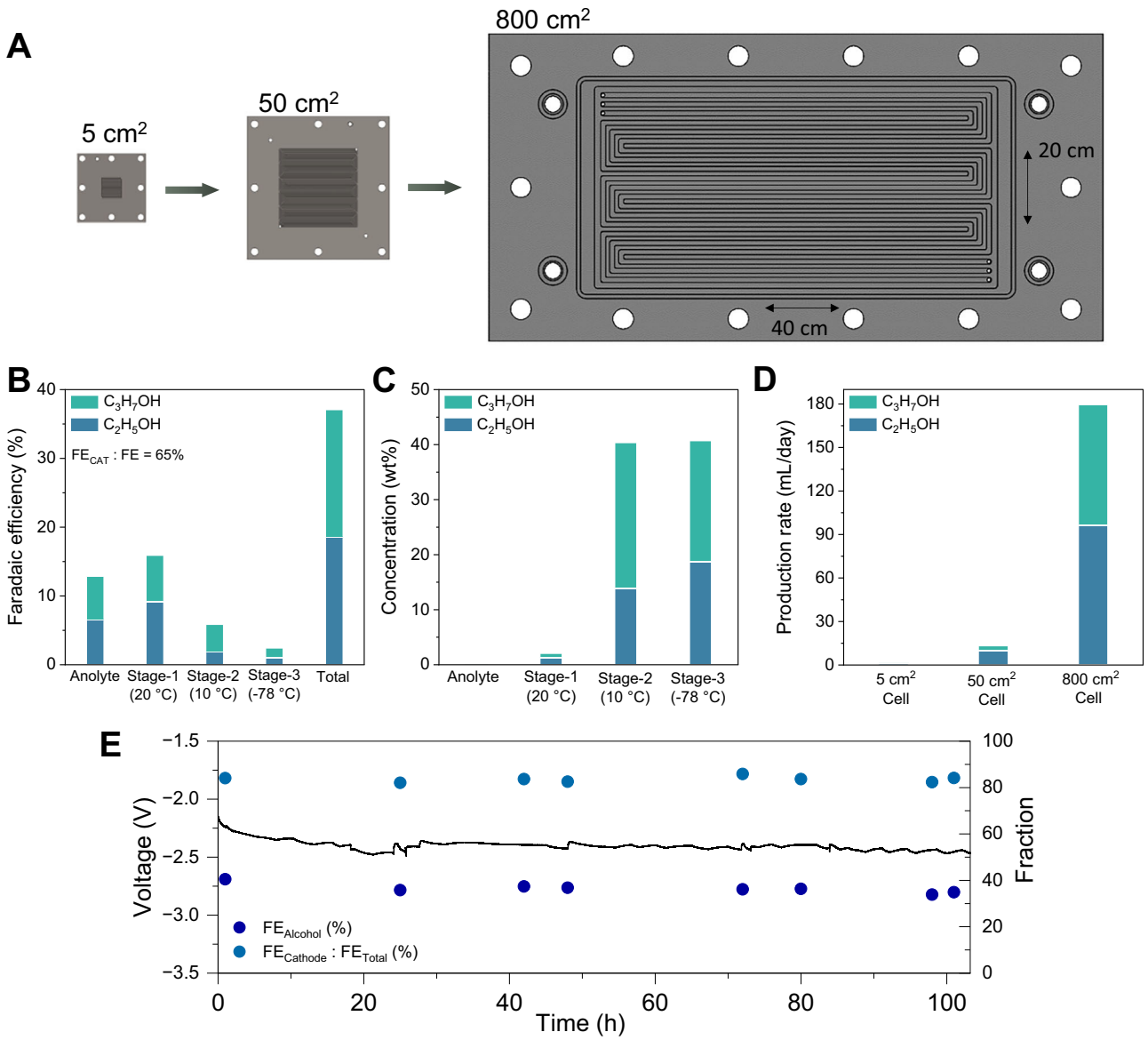

Fig. 4 | Demonstration of COR to alcohols in an 800 cm² electrolyzer at 80 A (100 mA/cm²). A Illustrations of the cathode electrode plates used for the 5 cm², 50 cm², and 800 cm² MEA electrolyzers. **B** Alcohol FE distribution from the 800 cm² electrolyzer collected from different locations. Stages-1/2/3 refer to the liquid outlets from the three condensers. **C** Concentration of alcohols collected from each location. **D** Comparison of the alcohol production rate from the 5 cm², 50 cm², and 800 cm² electrolyzers. **E** Stability test of the CEM MEA applied to the large-scale system with the 5 cm² cell at 100 mA cm⁻². Voltages represent the full-cell MEA potential and are not iR-corrected. Source data for the results are provided as a Source Data file.

Electrochemical measurements

The COR electrochemical measurements were performed in a 5 cm², 50 cm², or 800 cm² MEA cell with a stainless steel or titanium serpentine cathode flow field and a titanium serpentine anode flow field. The tests were all completed under ambient conditions. The cells were assembled by sandwiching a 254 µm-thick Nafion 1110 membrane (Fuel Cell Store) (in CEM experiments) or a 40 µm-thick PiperION-A40-HCO3 membrane (Versogen Inc.) (in AEM experiments) between a cathode and a Ir-mixed, metal oxide coated titanium felt anode (Magneto Special Anodes). The Nafion 1110 membrane was replaced by a Nafion 117 membrane for 800 cm² experiments due to the limited availability of Nafion 1110 in larger sizes. Nafion 115 was also evaluated. The membranes were treated according to the supplier specification. The 5 cm² and 50 cm² cells were sealed with a 250 µm silicone gasket on the cathode and a 1/16" viton o-ring on the anode side. The 800 cm² cell was sealed with a 3/16" buna o-ring. To maintain proper cooling in the 800 cm² electrolyzer, the electrolyte was circulated through a stainless-steel radiator with a fan, keeping the temperature constant at approximately 30 °C, as monitored by inline thermocouples throughout the experiment.

The CO stream was fed without humidification to the cell at 50 sccm with a mass-flow controller. Humidification of the CO gas was not required, as the water transported through the membrane was sufficient to support the COR reaction. A 1 M KOH anolyte was prepared by adding potassium hydroxide pellets (BioShop, PHY202) with deionized water prior to each test. The 1 M KOH anolyte was supplied to the anode at 10 mL/min with a peristaltic pump from a 200 mL container. The electrochemical measurements were performed with a potentiostat (Autolab PGSTAT204) equipped with a 10 A booster in galvanostatic mode or a power supply (Magna-Power SL series 10 V 250 A programmable DC power supply). The data was exported and processed in Excel. The cell was left for 1 h at each condition to accumulate liquid products. The cell voltages are all reported without iR-correction.

Electrochemical Impedance Spectroscopy

Electrochemical impedance spectroscopy (EIS) measurements were conducted on the 5 cm^2 cell using an EIS module (Autolab FRA32M) over a frequency range of 10^5 Hz to 1 Hz with an AC perturbation amplitude of 5 mA. The resulting Nyquist plots were analyzed using an equivalent circuit model (Supplementary Fig. 2). All experiments were conducted at ambient lab conditions (20 °C, 1 atm).

Product analysis

The COR gas products were analyzed with a gas chromatograph (Perkin Elmer Clarus 590) with a thermal conductivity detector (TCD) and a flame ionization detector (FID). The gas chromatograph was equipped with a Molecular Sieve 5 A Capillary Column and a packed Carboxen-1000 Column with argon as the carrier gas. The gas flowrates were measured with a bubble column or with a Coriolis mass flowmeter (Endress and Hauser).

The COR liquid products were measured using proton nuclear magnetic resonance spectroscopy ($1H^+$ NMR). The liquid products crossed-over to the anode side were obtained by taking samples from the anolyte. The cathode liquid products were obtained using either a liquid-collector or gas condenser applied downstream to the cathode gas outlet. The liquid-collector was a vial containing 10 mL of DI water held at 0°C with an ice bath, in which the cathode gas outlet was bubbled through to collect the liquid products. The condensers were glass spiral condensers that circulated water from an ice bath or isopropyl alcohol from a dry-ice bath to achieve the desired condensation temperatures. The samples were diluted with D_2O and DMSO was used as the internal standard. The analysis was performed with an Agilent DD2 500 spectrometer in water suppression mode.

The amount of alcohol crossover was measured by comparing the FE of the alcohols obtained from the vapor-phase in the cathode outlet gas to the total alcohol FE:

$$FE_{Cat} : FE_{Total} = \frac{EtOH\,FE_{Cathode} + PrOH\,FE_{Cathode}}{EtOH\,FE_{Cathode} + EtOH\,FE_{Anode} + PrOH\,FE_{Cathode}\,PrOH\,FE_{Anode}} \quad (1)$$

The FE of the liquid and gas products were calculated as follows:

$$FE_{Liquids} = n_i \times \frac{z_i F}{Q} \times 100\% \quad (2)$$

$$FE_{Gas} = x_i \times \upsilon \times \frac{z_i F P_0}{RTI} \times 100\% \quad (3)$$

Where n_i is the number of moles of each liquid product, F is the Faraday Constant, z_i is the number of electrons transferred for each product, Q is the total charge passed during liquid product collection, x_i is the volume fraction of each gas product, υ is the gas flowrate, P_0 is atmospheric pressure, R is the ideal gas constant, and T is the temperature.

Data availability

Data in tables is provided in the Supplementary Information. Source data are provided with this paper.

Code availability

All data and information for the simulations are available in the supplementary materials. Any additional information is available from the corresponding authors upon a reasonable request.

References

1. Bushuyev, O. S. et al. What should we make with CO_2 and how can we make it? *Joule* **2**, 825–832 (2018).
2. De Luna, P. et al. What would it take for renewably powered electrosynthesis to displace petrochemical processes? *Science* **364**, eaav3506 (2019).
3. Costentin, C., Robert, M. & Savéant, J.-M. Catalysis of the electrochemical reduction of carbon dioxide. *Chem. Soc. Rev.* **42**, 2423–2436 (2013).
4. Gattrell, M., Gupta, N. & Co, A. Electrochemical reduction of CO_2 to hydrocarbons to store renewable electrical energy and upgrade biogas. *Energy Convers. Manag.* **48**, 1255–1265 (2007).
5. Appel, A. M. et al. Frontiers, Opportunities, and challenges in biochemical and chemical catalysis of CO_2 fixation. *Chem. Rev.* **113**, 6621–6658 (2013).
6. Jouny, M., Luc, W. & Jiao, F. General Techno-Economic Analysis of CO_2 Electrolysis Systems. *Ind. Eng. Chem. Res.* **57**, 2165–2177 (2018).
7. Lark, T. J. et al. Environmental outcomes of the US Renewable Fuel Standard. *Proc. Natl Acad. Sci.* **119**, e2101084119 (2022).
8. Yang, D., Li, S., He, S. & Zheng, Y. Can conversion of CO_2 into fuels via electrochemical or thermochemical reduction be energy efficient and reduce emissions? *Energy Convers. Manag.* **273**, 116425 (2022).
9. Mo, W., Tan, X.-Q. & Ong, W.-J. Prospective life cycle assessment bridging biochemical, thermochemical, and electrochemical CO_2 reduction toward sustainable ethanol synthesis. *ACS Sustain. Chem. Eng.* **11**, 5782–5799 (2023).
10. Tan, X. & Nielsen, J. The integration of bio-catalysis and electrocatalysis to produce fuels and chemicals from carbon dioxide. *Chem. Soc. Rev.* **51**, 4763–4785 (2022).
11. Luo, T., Song, Q., Han, J., Li, Y. & Liu, L. The reduction of CO_2/bicarbonate to ethanol driven by Bio-electrochemical system using reduced graphene oxide modified nickel foam. *Sep. Purif. Technol.* **280**, 119437 (2022).
12. Luan, L. et al. Bioelectrocatalysis for CO_2 reduction: recent advances and challenges to develop a sustainable system for CO2 utilization. *Biotechnol. Adv.* **63**, 108098 (2023).
13. Shayesteh Zeraati, A. et al. Carbon- and energy-efficient ethanol electrosynthesis via interfacial cation enrichment. *Nat. Synth.* https://doi.org/10.1038/s44160-024-00662-x (2024).
14. Li, F. et al. Cooperative CO2-to-ethanol conversion via enriched intermediates at molecule–metal catalyst interfaces. *Nat. Catal.* **3**, 75–82 (2020).
15. Li, Y. C. et al. Binding site diversity promotes CO_2 electroreduction to ethanol. *J. Am. Chem. Soc.* **141**, 8584–8591 (2019).
16. Gu, Z. et al. Efficient electrocatalytic CO_2 reduction to C2+ alcohols at defect-site-rich Cu surface. *Joule* **5**, 429–440 (2021).
17. Wang, X. et al. Efficient electrically powered CO_2-to-ethanol via suppression of deoxygenation. *Nat. Energy* **5**, 478–486 (2020).
18. Verma, S., Kim, B., Jhong, H., Ma, S. C. & Kenis, P. J. A. A gross-margin model for defining technoeconomic benchmarks in the electroreduction of CO_2. *Chemsuschem* **9**, 1972–1979 (2016).
19. O'Brien, C. P. et al. CO_2 Electrolyzers. *Chem.Rev.* https://doi.org/10.1021/acs.chemrev.3c00206 (2024).
20. Robb, A. et al. Concentrated ethanol electrosynthesis from CO_2 via a porous hydrophobic adlayer. *ACS Appl. Mater. Interfaces* **14**, 4155–4162 (2022).
21. Salvatore, D. A. et al. Designing anion exchange membranes for CO_2 electrolysers. *Nat. Energy* **6**, 339–348 (2021).
22. Wang, N. et al. Suppressing the liquid product crossover in electrochemical CO_2 reduction. *SmartMat* **2** https://doi.org/10.1002/smm2.1018 (2021).
23. Zhang, J., Luo, W. & Züttel, A. Crossover of liquid products from electrochemical CO_2 reduction through gas diffusion electrode and anion exchange membrane. *J. Catal.* **385**, 140–145 (2020).
24. Barragán, V. M., Ruiz-Bauzá, C. & Mengual, J. I. On current dependence of the electro-osmotic permeability in ion-exchange membranes. *J. Membr. Sci.* **95**, 1–10 (1994).

25. Miao, R. K. et al. Electroosmotic flow steers neutral products and enables concentrated ethanol electroproduction from CO_2. *Joule* **5**, 2742–2753 (2021).
26. Greenblatt, J. B., Miller, D. J., Ager, J. W., Houle, F. A. & Sharp, I. D. The technical and energetic challenges of separating (photo)electrochemical carbon dioxide reduction products. *Joule* **2**, 381–420 (2018).
27. Xia, C. et al. Continuous production of pure liquid fuel solutions via electrocatalytic CO_2 reduction using solid-electrolyte devices. *Nat. Energy* **4**, 776–785 (2019).
28. Zhu, P. & Wang, H. High-purity and high-concentration liquid fuels through CO_2 electroreduction. *Nat. Catal.* **4**, 943–951 (2021).
29. Rabinowitz, J. A. & Kanan, M. W. The future of low-temperature carbon dioxide electrolysis depends on solving one basic problem. *Nat. Commun.* **11**, 5231 (2020).
30. Ma, M., Kim, S., Chorkendorff, I. & Seger, B. Role of ion-selective membranes in the carbon balance for CO_2 electroreduction via gas diffusion electrode reactor designs. *Chem. Sci.* **11**, 8854–8861 (2020).
31. Larrazábal, G. O. et al. Analysis of mass flows and membrane crossover in CO_2 teduction at high current densities in an MEA-Type electrolyzer. *ACS Appl. Mater. Interfaces* **11**, 41281–41288 (2019).
32. O'Brien, C. P. et al. Single Pass CO_2 conversion exceeding 85% in the electrosynthesis of multicarbon products via local CO_2 regeneration. *ACS Energy Lett.* **6**, 2952–2959 (2021).
33. Huang Jianan, E. et al. CO_2 electrolysis to multicarbon products in strong acid. *Science* **372**, 1074–1078 (2021).
34. Xu, Y. et al. A microchanneled solid electrolyte for carbon-efficient CO_2 electrolysis. *Joule* **6**, 1333–1343 (2022).
35. Ozden, A. et al. Carbon-efficient carbon dioxide electrolysers. *Nat. Sustain.* **5**, 563–573 (2022).
36. Küngas, R. Review—electrochemical CO_2 reduction for CO production: comparison of low- and high-temperature electrolysis technologies. *J. Electrochem. Soc.* **167**, 044508 (2020).
37. Ozden, A. et al. Cascade CO_2 electroreduction enables efficient carbonate-free production of ethylene. *Joule* **5**, 706–719 (2021).
38. Chen, R. et al. Highly selective production of ethylene by the electroreduction of carbon monoxide. *Angew. Chem. Int Ed. Engl.* **59**, 154–160 (2020).
39. Li, J. et al. Constraining CO coverage on copper promotes high-efficiency ethylene electroproduction. *Nat. Catal.* **2**, 1124–1131 (2019).
40. Ji, Y. et al. Selective CO-to-acetate electroreduction via intermediate adsorption tuning on ordered Cu–Pd sites. *Nat. Catal.* **5**, 251–258 (2022).
41. Luc, W. et al. Two-dimensional copper nanosheets for electrochemical reduction of carbon monoxide to acetate. *Nat. Catal.* **2**, 423–430 (2019).
42. Crandall, B. S. et al. Kilowatt-scale tandem CO_2 electrolysis for enhanced acetate and ethylene production. *Nat. Chem. Eng.* https://doi.org/10.1038/s44286-024-00076-8 (2024).
43. Terlouw, T., Bauer, C., McKenna, R. & Mazzotti, M. Large-scale hydrogen production via water electrolysis: a techno-economic and environmental assessment. *Energy Environ. Sci.* **15**, 3583–3602 (2022).
44. Smith, W. A., Burdyny, T., Vermaas, D. A. & Geerlings, H. Pathways to Industrial-Scale Fuel Out of Thin Air from CO2 Electrolysis. *Joule* **3**, 1822–1834 (2019).
45. Edwards, J. P. et al. Pilot-scale CO_2 electrolysis enables a semi-empirical electrolyzer model. *ACS Energy Lett.* **8**, 2576–2584 (2023).
46. Xu, H. et al. Highly selective electrocatalytic CO2 reduction to ethanol by metallic clusters dynamically formed from atomically dispersed copper. *Nat. Energy* **5**, 623–632 (2020).
47. Sun, W. P. et al. V-doped CuSe hierarchical nanotubes enabling flow-cell CO electroreduction to ethanol with high efficiency and selectivity. *Adv. Mater.* **34** https://doi.org/10.1002/adma.202207691 (2022).
48. O'Brien, C. P. et al. Scalability and stability in CO_2 reduction via tomography-guided system design. *Joule* **8**, 2903–2919 (2024).
49. Xu, Y., Xia, Z., Gao, W., Xiao, H. & Xu, B. Cation effect on the elementary steps of the electrochemical CO reduction reaction on Cu. *Nat. Catal.* **7**, 1120–1129 (2024).
50. Hou, J., Xu, B. & Lu, Q. Influence of electric double layer rigidity on CO adsorption and electroreduction rate. *Nat. Commun.* **15**, 1926 (2024).
51. Zhang, Z.-M. et al. Probing electrolyte effects on cation-enhanced CO2 reduction on copper in acidic media. *Nat. Catal.* **7**, 807–817 (2024).
52. Roschger, M. et al. Study on commercially available membranes for alkaline direct ethanol fuel cells. *ACS Omega* **8**, 20845–20857 (2023).
53. An, L. & Zhao, T. S. Performance of an alkaline-acid direct ethanol fuel cell. *Int. J. Hydrog. Energy* **36**, 9994–9999 (2011).
54. Adnan, M. A. et al. Directly-deposited ultrathin solid polymer electrolyte for enhanced CO_2 electrolysis. *Adv. Energy Mater.* **13**, 2203158 (2023).
55. Barique, M. A., Tsuchida, E., Ohira, A. & Tashiro, K. Effect of elevated temperatures on the states of water and their correlation with the proton conductivity of Nafion. *ACS Omega* **3**, 349–360 (2018).
56. Nelson, V. E. et al. Scaling CO2 electrolyzer cell area from bench to pilot. *ACS Appl. Mater. Interfaces* **16**, 50818–50825 (2024).

Acknowledgements

The authors acknowledge funding for this work from the Government of Canada's New Frontiers in Research Fund (NFRF), CANSTOREnergy project NFRFT-2022-00197. This work also received financial support from the Natural Sciences and Engineering Research Council of Canada (NSERC). D.S. acknowledges the support received from the Canada Research Chairs program. A.S. thanks NSERC for their support through postdoctoral fellowship.

Author contributions

D.S. supervised the project. C.P.O., P.P., and A.S.Z. conceived the ideas, performed the electrochemical experiments, analyses, and co-wrote the manuscript. P.P. and C.P.O. developed the downstream separation unit. C.P.O., S.L., and V.N. developed and tested the scaled electrolyzer. A.P. and J.W. performed the cost separation analysis. S.P., Y.C.X., R.D., P.H,. and R.K.M. assisted with the development of the electrolyzer and catalyst. D.S., C.M.G., N.W., R.K.M., and E.H.S. contributed to the manuscript editing and the discussions. D.S. supervised the work. All authors participated in result discussions and assisted with paper preparation.

Competing interests

The authors declare no competing interests.

Additional information

Supplementary information The online version contains supplementary material available at https://doi.org/10.1038/s41467-025-59180-9.

Correspondence and requests for materials should be addressed to Ali Shayesteh Zeraati or David Sinton.

Peer review information *Nature Communications* thanks Woong Hee Lee, Peyman Taheri, and the other, anonymous, reviewer(s) for their contribution to the peer review of this work. A peer review file is available.